Physics Letters B 775 (2017) 190–195

Contents lists available at ScienceDirect

Physics Letters B

www.elsevier.com/locate/physletb

Kinetic energy dependence of fission fragment isomeric ratios for spherical nuclei ^{132}Sn

A. ChebbouBi [a,b,*], G. Kessedjian [b], O. Litaize [a], O. Serot [a], H. Faust [c], D. Bernard [a], A. Blanc [c], U. Köster [c], O. Méplan [b], P. Mutti [c], C. Sage [b]

[a] CEA, DEN, DER, SPRC, Cadarache, Physics Studies Laboratory, F-13108 Saint-Paul-lès-Durance, France
[b] LPSC, Université Grenoble-Alpes, CNRS/IN2P3, F-38026 Grenoble Cedex, France
[c] Institut Laue-Langevin, F-38042 Grenoble Cedex 9, France

ARTICLE INFO

Article history:
Received 16 October 2017
Received in revised form 27 October 2017
Accepted 27 October 2017
Available online 31 October 2017
Editor: D.F. Geesaman

Keywords:
Isomeric ratio
Mass spectrometer
Angular momentum distribution
Fission fragment

ABSTRACT

Isomeric ratios are a powerful observable to investigate fission fragment total angular momenta. A recent experimental campaign achieved at the LOHENGRIN spectrometer, shows a kinetic energy dependence of µs isomeric ratios from fission fragments populated in neutron induced fission of ^{235}U. For the first time, this dependence was measured for the isomeric ratio of the doubly magic ^{132}Sn. A Bayesian assessment of the angular momentum distribution of ^{132}Sn is proposed according to calculations performed with the FIFRELIN code and interpreted with spin generation models.

1. Introduction

Seven decades after its discovery [1,2], the accurate understanding of the fission process is still one of the significant challenges faced in nuclear physics. A multitude of fission models has been developed to reproduce and explain the experimental results through different hypotheses. Some are based on a microscopic approach, i.e. the solution of a quantum mechanical description, either through an effective force [3], or using an energy potential based on a macroscopic model [4,5]. In contrast, the statistical model [6,7] refers to a thermodynamic equilibrium at the scission point. We can also mention scission point models [8] which are based on the energy balance at the scission point or liquid drop models [9] which consider the evolution of the compound nucleus as a liquid drop and evaluate its potential energy. Finally the phenomenological approach [10] describes the fission process as a competition between several modes. This incomplete list shows how different strong hypotheses can lead to a description of the same process. Some models take into account a dynamical description whereas others are static. However, until now, fission yields and emitted prompt particle observables cannot be predicted with an acceptable accuracy by fission models.

In this respect the dynamical aspects of the fission process may be recognized as a necessary ingredient [3]. The spin distribution of a fragment could be a remnant of the dynamical effects from the saddle point to the scission point [11]. This is an important issue, in particular for the spherical nuclei at scission. To assess this quantity, an indirect method through isomeric ratio (IR) measurements was used. In the following, IR refers to the ratio of the independent fission yield of the isomer over the sum of the independent yields of ground state and isomer. This observable is of interest because it preserves the initial spin information resulting from the fission process just after the prompt particle emission [12–14]. Moreover as shown by Regnier et al. [15], modeling the multiplicities and spectra of prompt neutron and γ emissions requires an accurate knowledge of the fission fragment spin distribution. These information are mandatory in the calculation of γ heating and damage of nuclear reactor components [16]. In order to design the next generation of nuclear reactors with a higher level of confidence, improvements in both theoretical and experimental sides must be achieved.

Previous measurements of IRs were summarized by Naik et al. [17] and Stetcu et al. [18] who were able to deduce a spin distribution per fission fragment characterized by the $J_{\rm rms}$ parameter, which is associated to a spin cut-off parameter. The data from [17]

* Corresponding author at: CEA, DEN, DER, SPRC, Cadarache, Physics Studies Laboratory, F-13108 Saint-Paul-lès-Durance, France.
E-mail address: abdelhazize.chebbouBi@cea.fr (A. Chebbouhi).

https://doi.org/10.1016/j.physletb.2017.10.067
0370-2693/

point out an odd–even effect on $J_{\rm rms}$ [17]. The authors state that fission fragment angular momentum is related to the fragment deformation. Note that the more common odd–even effect in the isotopic yields decreases as the fissility increases. This strong correlation highlights the role of the intrinsic excitation energy [19]. However the $J_{\rm rms}$ odd–even effect was found to be independent of the fissioning system, minimizing the role of the intrinsic excitation energy. These observations question the part of the deformation energy in the spin generation.

Former experiments [20,21] have shown a slight dependence of IRs on kinetic energy as predicted by collective excitation models [22,23], the orientation pumping mechanism [24] and the statistical model of fission [12]. A more recent measurement [14] at the LOHENGRIN spectrometer of the Institut Laue-Langevin was specifically aimed to study IRs at the highest and lowest accessible kinetic energies. According to [25] et al., these regions correspond to the compact and deformed cold configurations respectively. This experiment found a slight indication for a drop of the IRs at very low kinetic energy of the fission product. This would suggest that another spin generation mechanism has to be added to the so-called wriggle and bending modes [9], which describe collective excitations. Namely thermal excitation of single particle states of the nucleus seems to be involved in the process of spin generation in spherical and near-spherical nuclei. In order to corroborate and extend these observations, new measurements of IRs, as a function of the kinetic energy, were performed at the LOHENGRIN spectrometer. Also, for the first time, IR measurements on doubly magic ^{132}Sn were achieved and a particular attention was given to the systematic errors of the experiment.

In this letter, we report measured IRs of ^{132}Sn after neutron evaporation populated in thermal neutron induced fission of ^{235}U. These data provide sensitive tests for different theoretical models of nuclear level densities, γ strength functions and also provide a hint to the mechanism involved in the angular momentum generation in fission.

2. Experimental setup

The LOHENGRIN recoil separator for fission products [26] is located at the high-flux reactor of Institut Laue-Langevin (ILL) in Grenoble, France. The fission target is placed in an evacuated beam tube, at a thermal neutron flux of about 5×10^{14} n cm^{-2} s^{-1}. The fission target (91 µg cm^{-2} of ^{235}U) is covered by a sputtered Ta layer (195 µg cm^{-2}) to reduce self-sputtering of the actinide target and to obtain a better control of its burn-up behavior [27]. Since IRs are relative measurements, no correction of the time evolution of the target is needed.

The spectrometer is made up of a horizontal magnetic deflection followed by a vertical electrostatic deflection. A focusing magnet, the Reverse Energy Dispersion (RED) magnet increases the particle density at the focal plane position [28]. The combination of a magnetic field and an electric field allows the separation of fission fragments according to the ratios of their kinetic energy over their ionic charge and their mass over their ionic charge. The variable energy acceptance of LOHENGRIN was set to 2.5% in this experiment.

An ionization chamber (IC) was placed in the focal plane to detect the incoming ions. These lose about one third of their kinetic energy in 20 cm of isobutane at 15 mbar before being implanted into an aluminum foil. Two clover detectors consisting of four high purity germanium (Ge) crystals each were placed adjacent to the IC at the height of the stopper foil. Signals from the IC and the Ge detectors were recorded with a trigger-less digital data acquisition.

3. Data analysis

The data were analyzed off-line. Ion-gated γ spectra were produced by sorting γ events recorded within a time gate of about 10 $T_{1/2}^{\rm isomer}$ after an incoming ion providing an IC signal. These ion-gated spectra were used to measure the isomeric state population. The gated spectra are very clean since the background only comes from rare fortuitous events. The measurement of the ground state, which decays by $\beta\gamma$, was done by extracting its γ lines from the ungated spectra. Because of the background coming from different separated nuclei and the ambient background, the statistical uncertainty associated to the ground state quantification was larger than the one for the isomeric state. Each measurement corresponds to a five hours run. Fig. 1 shows a gated γ spectrum and the associated time spectrum of ^{132m}Sn. The lifetime derived is compatible with literature (see Table 1).

The different γ lines used for this analysis are summarized in Table 1. The decay properties are obtained from Ref. [29]. A MCNP [30] simulation was performed to assess the relative detection efficiency of the Ge detectors. This simulation was validated with experimental data points from a ^{60}Co point source and an extended ^{134}Te source obtained by ion-implantation on the aluminum foil. For the region of interest, 100–1000 keV, the simulated efficiencies reproduced the measured ones to better than 2.5%.

The IR for a selected kinetic energy E_k corresponds to the ratio of the isomeric state over the total (i.e. sum of isomer and ground state) of this nuclide populated by the fission process. To deduce IRs from count rates, one important step is the solution of the Bateman equations. Here, the IRs at the fission target, after neutron evaporation, are obtained by correcting for the decay losses during the flight time through the 23 m long spectrometer.

To evaluate precisely the IRs and their related uncertainties, a Total Monte Carlo propagation of uncertainties was applied. Since some parameters are involved in different corrections, an analytic calculation of the uncertainty would have been very difficult. The

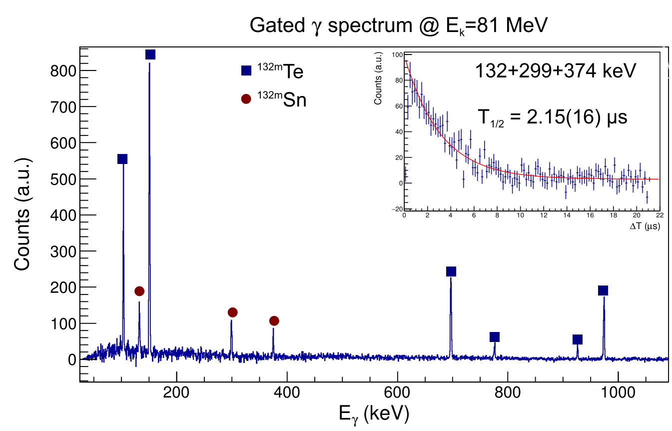

Fig. 1. (Color online.) 20 µs gated γ spectrum for ^{132}Sn at kinetic energy E_k = 81 MeV. Since the LOHENGRIN spectrometer only selects masses, isomeric states of ^{132}Te can also be seen. By selecting only few γ lines, the lifetime of the ^{132m}Sn can be derived as shown in the insert.

Table 1
Nuclear structure and decay data used for the analysis [29]. Lifetime and spin parity of isomeric and ground state level are also indicated.

^{132m}Sn (2.03(4) µs) $J^\pi = 8^+$		^{132}Sn (39.7(8) s) $J^\pi = 0^+$	
E_γ (keV)	I_γ (absolute)	E_γ (keV)	I_γ (absolute)
132.3(3)	62.657	246.87(5)	42.0(22)
299.2(3)	96.544	340.53(5)	48.8(12)
374.3(3)	84.2(24)	899.04(5)	44(3)
		992.66(8)	36.6(21)

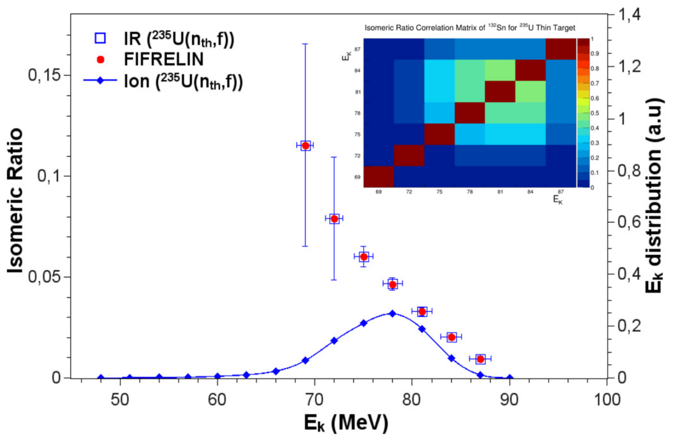

Fig. 2. (Color online.) Dependence of ^{132}Sn IR on the kinetic energy selected by the LOHENGRIN spectrometer for a ^{235}U target. Blue line corresponds to the kinetic energy distribution of the mass 132 (right axis). Open squares are the experimental data. Red circles represent FIFRELIN calculations with the best spin cut-off parameter value (see text for details). On the up-right side, experimental correlation matrix of $IR(E_k)$ is shown.

principle of this method is to sample simultaneously all independent parameters used in the analysis. Stated differently, all the independent parameters are considered as random variables with known mean and standard deviation values. Every independent parameter was considered as normally distributed. These parameters are count rates extracted from the γ spectra, relative intensity of each γ line, their detection efficiency, the normalization factor to get an absolute value of these intensities, the branching ratio, the lifetime, the kinetic energy, the spectrometer flight time and the measurement time. The covariance matrix between the different measurements was also computed. With this method, the probability density function of the IRs can be built in addition to the mean value and its uncertainty.

For each sampling of a given parameter (the other ones are kept fixed) an IR is deduced. A fitting method is used to obtain the derivative term involved in the sensibility, which is needed to calculate the correlation coefficients:

$$\begin{aligned}
&IR_i(E_k) = IR_i = f\left(\{a_l\}\right)\\
&S_{il} = \frac{\partial f_i}{\partial a_l}\frac{\overline{a_l}}{f\left(\{\overline{a_l}\}\right)}\\
&\frac{\mathrm{Cov}\left(IR_i, IR_j\right)}{IR_i IR_j} = \sum_l S_{il}S_{jl}\frac{\sigma_{a_l}^2}{a_l^2}
\end{aligned} \tag{1}$$

with f a function which links all the parameters $\{a_l\}$, S_{il} the sensibility of the ith measurement to the lth parameter, Cov the covariance matrix and σ_{a_l} the uncertainty of the parameter a_l.

The correlation matrix reveals the weight of the systematic uncertainty compared to the standard deviation of each measurement. Here, systematic uncertainties are between 3% and 4% whereas statistical uncertainties range from 4% to 40%. Therefore the correlation is between 1% and 45% (see Fig. 2).

Fig. 2 illustrates IR measurements of ^{132}Sn as a function of the kinetic energy selected by the LOHENGRIN spectrometer (E_k) i.e. without any energy loss correction. Indeed it is complex to correct the measured kinetic energy from the energy loss through the target and its cover. Such corrections require taking into account the time and temperature evolution of the target heterogeneity which are difficult to predict *in situ*. Therefore we present here the energies "as measured", i.e. not corrected for these losses. Nevertheless, a pronounced dependence on the kinetic energy was observed as illustrated in Fig. 2. It must be noted that target thickness has a huge impact on the slope of the $IR(E_K)$. This effect will be discussed with more details in a further paper. Finally the correlation matrix is plotted and reveals that uncertainties mainly come from statistics. In other words, uncertainties coming from the ^{132}Sn level scheme are low. Therefore the uncertainty of the mean value (weighted by the kinetic energy distribution) is mainly governed by the statistical uncertainty (see Table 2). Note that a measurement was performed at 66 MeV but no signal was seen. Then, a limit of detection for both isomeric and ground state, was derived. Unfortunately because of the IR definition, it is impossible to compute a limit of detection for this observable.

Table 2
Determination of the mean IR with its uncertainties considering or not the correlation terms.

$\overline{IR}$	σ^{stat}	σ^{tot} (w/o corr.)	σ^{tot} (w/ corr.)
0.0541	0.0058	0.0072	0.0074

4. From IR to J_{rms} using FIFRELIN

To go further and compare our experimental results with theoretical spin generation calculations, one has to derive an angular momentum distribution. Note that the method described in the following, in order to extract a spin cut-off parameter, is independent of the Total Monte Carlo experimental analysis method employed in the IR evaluation. To extract a fission fragment spin distribution, a γ de-excitation code is required. This tool would permit to answer the question: "What are the fission fragment states (E^*, J^π) which lead to the measured isomeric ratios (post neutron emission)?". For that, we use FIFRELIN (FIssion FRagment Evaporation Leading to an Investigation of Nuclear data) [31,32] which is a Monte Carlo code simulating the prompt fission neutron and γ-ray emission. It allows to calculate fission observable distributions related to prompt neutrons, prompt γ-rays, prompt electrons and fission fragments. In this work, the starting point is not the scission point but a given initial state of excitation energy and angular momentum $\left(E^*, J^\pi\right)$ of the nucleus of interest. FIFRELIN is then used only as a nuclear de-excitation code and does not use any spin generation model at scission. In this framework the important points to simulate this de-excitation are the modeling of nuclear level density, γ strength function and the nuclear level scheme at low energy.

When excitation energy increases, statistical models are needed to describe the nuclear level density. We employed the Constant Temperature Model (CTM) in this work. It describes an exponential evolution of the number of nuclear states as a function of excitation energy. The CTM is known to work well at low excitation energy [33,34] (below several MeV typically). The Enhanced Generalized LOrentzian model (EGLO) [35] was used for the γ strength function. This function is related to the probability for an initial state to decay towards a given final state. At low energies ($E^* < E_{\text{cut}} = 4.94$ MeV) the experimental level scheme and related γ-ray intensities, provided by the RIPL-3 database [36,37] are considered. The scheme is supposed to be fully known up to E_{cut}. Above E_{cut} FIFRELIN completes the partial experimental level scheme with a nuclear level density model [32].

To resume, for a given initial state $\left(E^*, J^\pi\right)$ the probability to feed the isomer and the ground states is calculated through the combination of a nuclear level density model, experimental level scheme and a γ strength function. For each excitation energy, from the isomeric state to the neutron binding energy, and each J^π (from $0^\pm$ to $30^\pm$) an IR is calculated. The results are averaged according to the most commonly used distribution [see Eq. (2)] in

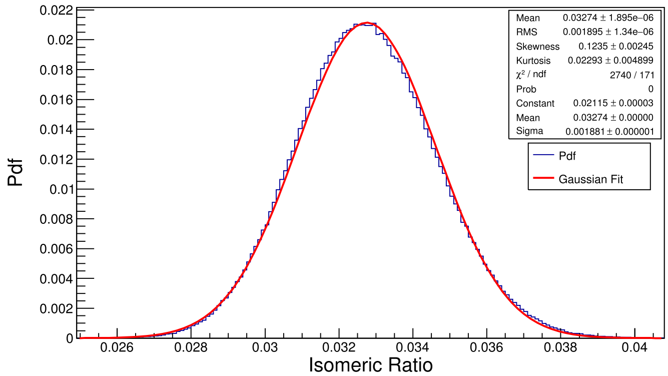

Fig. 3. (Color online.) Blue histogram represents the probability density function of the IR measured at $E_k = 81$ MeV obtained by the Total Monte Carlo calculation. It is fitted by a Gaussian function (red line). A slight difference can be seen (which is reflected by the poor χ^2 value). Nevertheless, the mean value and the standard deviation from the histogram are then used in the likelihood [see eq. (3)], which assumes a Gaussian behavior of variables.

order to compare them with experimental data:

$$IR_{\mathrm{FIF}}\left(E^*, J_{\mathrm{rms}}\right) = \sum_J \sum_\pi P(\pi) P(J) IR_{\mathrm{FIF}}\left(E^*, J^\pi\right) \tag{2}$$

$$\text{with } P(\pi) = P(\pm 1) = \frac{1}{2}$$

$$\text{and } P(J) \propto (2J+1) \exp\left(-\frac{(J+1/2)^2}{J^2_{\mathrm{rms}}}\right)$$

where J_{rms} is related to an effective moment of inertia and represents a spin cut-off parameter [19].

An indicator based on a Bayesian approach was built to evaluate the best J_{rms} parameter in the (E^*, J_{rms}) space that reproduces our experimental results. A Gaussian distribution of our measurements is assumed, which is quite a validated hypothesis as shown in Fig. 3.

The likelihood can be expressed as follows:

$$\mathcal{L}\left(E^*, J_{\mathrm{rms}}|E_k\right) \propto \exp\left(-\frac{\left(IR_{\mathrm{exp}}\left(E_k\right) - IR_{\mathrm{FIF}}\left(E^*, J_{\mathrm{rms}}\right)\right)^2}{2\left(\sigma^2_{\mathrm{exp}} + \sigma^2_{\mathrm{FIF}}\right)}\right) \tag{3}$$

This assessment is only relevant if the experimental results can be reproduced [38,39]. This statement is illustrated in Fig. 2 where the results of the comparison between the ^{132}Sn experimental IR and the calculated ones with FIFRELIN is shown.

The Bayesian probability as a function of E^* and J_{rms} ($\mathcal{L}(E^*, J_{\mathrm{rms}}|E_k)$) is shown on Fig. 4(a) for the experimental IR at $E_k = 81$ MeV. It represents the de-excitation path in the (E^*, J_{rms}) space which can reproduce experimental IRs. This probability allows us to determine the mean J_{rms}, its standard deviation and the best value of J_{rms} (which corresponds to the maximum value of the Bayesian indicator) as a function of the kinetic energy [see Fig. 4(b)]. No prior assumption was used in the analysis. In other words all hypotheses have the same initial probability. The large uncertainty from the low kinetic energy points is coming from the important experimental statistical uncertainty. Nevertheless a clear dependence between J_{rms} and the kinetic energy is observed. The obtained result points out that even without a good knowledge of experimental excitation energy, the correlation between the spin cut-off parameter and the kinetic energy is observed. Taking into account additional considerations (experimental or theoretical) on the excitation energy as a function of kinetic energy, a better constraint on J_{rms} would be achieved. Finally it is also possible to combine all experimental data and extract the mean value $\overline{J_{\mathrm{rms}}} = 4.60 \pm 0.20\ \hbar$ from $\overline{IR}$ and the associated Bayesian probability $\mathcal{L}\left(E^*, \overline{J_{\mathrm{rms}}}|\overline{IR}\right)$.

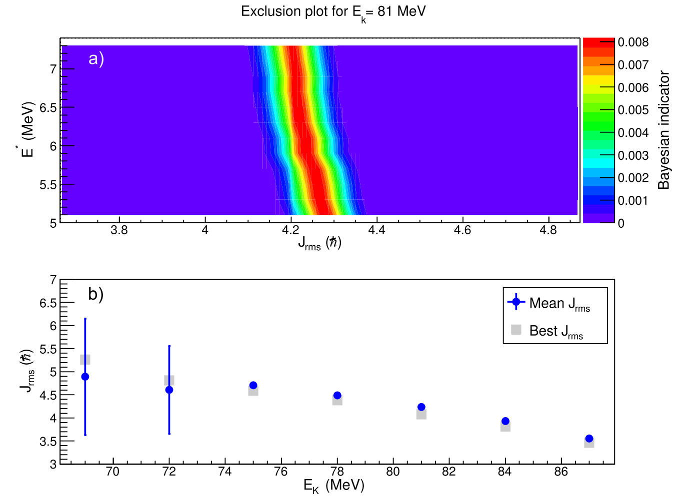

Fig. 4. (Color online.) (a) Bayesian probability in the (E^*, J_{rms}) space e.g. $\mathcal{L}(E^*, J_{\mathrm{rms}}|E_k)$, given by comparing FIFRELIN calculations and the experimental IR at $E_k = 81$ MeV for ^{132}Sn. The upper limit of excitation energy is close to the neutron binding energy ($S_n = 7.3$ MeV) whereas the lower limit is close to the level energy of the isomeric state ($E = 4.8$ MeV). (b) For each experimental kinetic energy, two estimations of J_{rms} were derived: the mean value weighted by the Bayesian probability $\mathcal{L}(E^*, J_{\mathrm{rms}}|E_k)$ and the best value associated to the highest Bayesian probability (a). A clear dependence of the J_{rms} with kinetic energy is highlighted.

5. Discussion

It is clear that for the doubly magic ^{132}Sn a dependence of IRs and J_{rms} as a function of kinetic energy is observed [see Figs. 2 and 4(b)]. These observations lead to the following considerations:

i) Considering spherical shape of the nucleus and according to the bending and wriggle modes and the pumping mechanism, the fragment spin is expected to be equal to zero [24,22,23,14]. However, our measurements clearly find a non-zero value. Thus, following these models, a slightly deformed ^{132}Sn at scission must be assumed, which seems to be unrealistic.

ii) Considering, at the scission point, no deformation of ^{132}Sn, this dependence could highlight the impact of the dynamics of the fission process. In other words, the spin generation could appear during the descent from the saddle to the scission point [3,11]. It is also possible that in such configuration (spherical shape of the nucleus) the complementary fragment, which is supposed deformed, may play a significant role in the generation of the spin of both fragments. Indeed, the kinetic energy distribution can be explained by the deformation of the complementary fragment. At higher kinetic energy, the light fragment is supposed spherical whereas at lower kinetic energy it is considered largely deformed. Then a strong correlation between the isomeric ratio (and the derived J_{rms}) and the complementary fragment deformation may exist.

iii) The statistical model describes a one-step process from an initial to a final state where the probability of excitation is given by the level density of the final state [40,12]. Any deformed quantum state enters only indirectly via the level density. All the characteristics involved in the fission process, in particular the spin generation, are then governed by the phase space available at the scission point [6]. Since the spin cut-off parameter is related to the temperature [41], J_{rms} can then be derived from the total excitation energy at scission [12]. No more dependence on deformation energy of the nucleus is required to explain a decrease of the spin cut-off parameter with the increase of the kinetic energy.

iv) According to the thermal excitation of single particle states, the spin cut-off parameter is expected to be small for compact (high kinetic energy) and deformed (low kinetic energy) cold configurations [14]. In such configurations, intrinsic energy is supposed to be null, which are the consequences of the competition between deformation energy and Coulomb energy [25]. Because of the relatively high background, for both isomeric and ground state, it was not possible to extract IR at lower kinetic energy (e.g. 66 MeV) and then test more deeply this hypothesis.

Results on ^{132}Sn permit to go further and highlight the limit of the knowledge on this subject. Nevertheless, this article does not have the ambition to validate any specific models, but to bring new experimental results to better constrain them. In this scheme ^{132}Sn is particularly appropriate to do a stress test on the validity of the hypothesis discussed previously. Further theoretical calculations are required to test more precisely the assumption of different models.

6. Conclusion and outlook

For the first time, the dependence of IRs with kinetic energy was measured for the doubly magic ^{132}Sn produced by thermal neutron induced fission of ^{235}U. Covariance matrix and probability density functions of measurements were computed and used to deduce the J_{rms} from this Bayesian statistical analysis. Calculations from FIFRELIN, with CTM as nuclear level density and EGLO as γ strength function were performed to derive a J_{rms} from the data. This nucleus is a test case to validate the assumption made in any theoretical calculation of the fission process.

These observations underline the need of new measurements of IRs as a function of the kinetic energy. A new measurement campaign is under way at the ILL during which different fissioning systems and different µs isomers, with different excitation energies will be studied. An even more complete picture can be obtained by prompt γ-ray spectroscopy in coincidence with energy resolved fission fragment tagging. This is a key objective of the FIPPS instrument [42], thus enabling a complete test of fission, nuclear level density and γ strength function models.

Acknowledgements

This work was supported by IN2P3, by the University of Grenoble Alpes and by “le défi NEEDS”. The authors are grateful for the support of the ILL and all the staff involved from CEA-Cadarache and LPSC.

References

[1] O. Hahn, F. Strassmann, Über den nachweis und das verhalten der bei der bestrahlung des urans mittels neutronen entstehenden erdalkalimetalle, Naturwissenschaften 27 (1) (1939) 11–15.
[2] L. Meitner, O.R. Frisch, Disintegration of uranium by neutrons: a new type of nuclear reaction, Nature 143 (3615) (1939) 239–240.
[3] H. Goutte, J.F. Berger, P. Casoli, D. Gogny, Microscopic approach of fission dynamics applied to fragment kinetic energy and mass distributions in ^{238}U, Phys. Rev. C 71 (2005) 024316.
[4] P. Möller, A.J. Sierk, A. Iwamoto, Five-dimensional fission-barrier calculations from ^{70}Se to ^{252}Cf, Phys. Rev. Lett. 92 (2004) 072501.
[5] J. Randrup, P. Möller, Brownian shape motion on five-dimensional potential-energy surfaces: nuclear fission-fragment mass distributions, Phys. Rev. Lett. 106 (2011) 132503.
[6] T. Ericson, The statistical model and nuclear level densities, Adv. Phys. 9 (36) (1960) 425–511.
[7] P. Fong, Statistical theory of nuclear fission: asymmetric fission, Phys. Rev. 102 (1956) 434–448.
[8] B.D. Wilkins, E.P. Steinberg, R.R. Chasman, Scission-point model of nuclear fission based on deformed-shell effects, Phys. Rev. C 14 (1976) 1832–1863.
[9] J.R. Nix, W.J. Swiatecki, Studies in the liquid-drop theory of nuclear fission, Nucl. Phys. 71 (1) (1965) 1–94.
[10] U. Brosa, S. Grossmann, A. Müller, Nuclear scission, Phys. Rep. 197 (4) (1990) 167–262.
[11] J.B. Wilhelmy, E. Cheifetz, R.C. Jared, S.G. Thompson, H.R. Bowman, J.O. Rasmussen, Angular momentum of primary products formed in the spontaneous fission of ^{252}Cf, Phys. Rev. C 5 (1972) 2041–2060.
[12] H. Faust, U. Köster, T. Materna, W. Urban, Population characteristics for spin and excitation energy of fragments in thermal neutron induced fission, J. Korean Phys. Soc. 59 (2) (2011) 879–882.
[13] R. Vandenbosch, J. Huizenga, Nuclear Fission, Academic Press, New York–London, 1973.
[14] F. Gönnenwein, I. Tsekhanovich, V. Rubchenya, Angular momenta of near-sperical fission fragments, Int. J. Mod. Phys. E 16 (2) (2007) 410–424.
[15] D. Regnier, O. Litaize, O. Serot, Preliminary results of a full Hauser–Feshbach simulation of the prompt neutron and gamma emission from fission fragments, Phys. Proc. 47 (0) (2013) 47–52.
[16] G. Rimpault, D. Bernard, D. Blanchet, C. Vaglio-Gaudard, S. Ravaux, A. Santamarina, Needs of accurate prompt and delayed γ-spectrum and multiplicity for nuclear reactor designs, Phys. Proc. 31 (0) (2012) 3–12.
[17] H. Naik, S.P. Dange, R.J. Singh, Angular momentum of fission fragments in low energy fission of actinides, Phys. Rev. C 71 (2005) 014304.
[18] I. Stetcu, P. Talou, T. Kawano, M. Jandel, Isomer production ratios and the angular momentum distribution of fission fragments, Phys. Rev. C 88 (2013) 044603.
[19] C. Wagemans, The Nuclear Fission Process, CRC Press, 1991.
[20] J. Bocquet, F. Schussler, E. Monnand, K. Sistemich, Effect of fragment kinetic energy on the supply of isomeric states in ^{236}U fission, in: IAEA (Ed.), Proc. Symp. Physics and Chemistry of Fission 1979, vol. 2, 1980, pp. 179–191.
[21] H. Denschlag, H. Braun, W. Faubel, Distribution of nuclear charge and angular momentum in chains 132–137, 99, and 102 of $^{235}U(n_{th}, f)$ at various kinetic energies and ionic charge states of the fragments, in: IAEA (Ed.), Proc. Symp. Physics and Chemistry of Fission 1979, vol. 2, 1980, pp. 153–177.
[22] J. Rasmussen, W. Nörenberg, H. Mang, A model for calculating the angular momentum distribution of fission fragments, Nucl. Phys. A 136 (2) (1969) 465–480.
[23] M. Zielinska-Pfabé, K. Dietrich, Angular momentum distribution of fission fragments as a result of bending modes at the scission point, Phys. Lett. B 49 (2) (1974) 123–128.
[24] L. Bonneau, P. Quentin, I.N. Mikhailov, Scission configurations and their implication in fission-fragment angular momenta, Phys. Rev. C 75 (2007) 064313.
[25] T. Thomas, W. Gibson, G. Safford, Thermal neutron induced fission of ^{235}U, ^{233}U and ^{239}Pu, in: IAEA (Ed.), Proc. Symp. Physics and Chemistry of Fission 1965, vol. 1, 1965, pp. 467–480.
[26] P. Armbruster, M. Asghar, J. Bocquet, R. Decker, H. Ewald, J. Greif, E. Moll, B. Pfeiffer, H. Schrader, F. Schussler, G. Siegert, H. Wollnik, The recoil separator lohengrin: performance and special features for experiments, Nucl. Instrum. Methods 139 (0) (1976) 213–222.
[27] U. Köster, H. Faust, T. Materna, L. Mathieu, Experience with in-pile fission targets at LOHENGRIN, Nucl. Instrum. Meth. A 613 (3) (2010) 363–370.
[28] G. Fioni, H. Faust, M. Gross, M. Hesse, P. Armbruster, F. Gönnenwein, G. Münzenberg, Reduction of energy dispersion on a parabola mass spectrometer, Nucl. Instrum. Meth. A 332 (1–2) (1993) 175–180.
[29] Y. Khazov, A. Rodionov, S. Sakharov, B. Singh, Nuclear data sheets for, Nucl. Data Sheets 104 (3) (2005) 497–790.
[30] X-5 MCNP Team, MCNP5 1.40, LA-UR-05-8617, 2005.
[31] O. Litaize, O. Serot, Investigation of phenomenological models for the monte carlo simulation of the prompt fission neutron and γ emission, Phys. Rev. C 82 (2010) 054616.
[32] D. Regnier, O. Litaize, O. Serot, An improved numerical method to compute neutron/gamma deexcitation cascades starting from a high spin state, Comput. Phys. Commun. 201 (2016) 19–28.
[33] K.-H. Schmidt, B. Jurado, Entropy driven excitation energy sorting in superfluid fission dynamics, Phys. Rev. Lett. 104 (2010) 212501.
[34] T. von Egidy, D. Bucurescu, Statistical nuclear properties (level densities, spin distributions), J. Phys.: Conf. Ser. 338 (1) (2012) 012028.
[35] J. Kopecky, M. Uhl, Test of gamma-ray strength functions in nuclear reaction model calculations, Phys. Rev. C 41 (1990) 1941–1955.
[36] R. Capote, M. Herman, P. Obložinský, P. Young, S. Goriely, T. Belgya, A. Ignatyuk, A. Koning, S. Hilaire, V. Plujko, M. Avrigeanu, O. Bersillon, M. Chadwick, T. Fukahori, Z. Ge, Y. Han, S. Kailas, J. Kopecky, V. Maslov, G. Reffo, M. Sin, E. Soukhovitskii, P. Talou, RIPL – reference input parameter library for calculation of nuclear reactions and nuclear data evaluations, Nucl. Data Sheets 110 (12) (2009) 3107–3214.
[37] M. Verpelli, R. Capote, Update of RIPL nuclear levels segment, International Nuclear Data Committee INDC(NDS)-0702.

[38] J. Neyman, E.S. Pearson, On the problem of the most efficient tests of statistical hypotheses, Phil. Trans. R. Soc. A 231 (694–706) (1933) 289–337.
[39] G. Kessedjian, O. Méplan, A. Billebaud, R. Brissot, S. Chabod, V. Ghetta, M. Heusch, E. Liatard, ^{7}Li neutron-induced elastic scattering cross section measurement using a slowing-down spectrometer, EPJ Web Conf. 8 (2010) 07005.
[40] H.R. Faust, Z. Bao, Higher moments in the kinetic energy distribution of fission products, Nucl. Phys. A 736 (1–2) (2004) 55–76.
[41] A. Gilbert, A. Cameron, A composite nuclear-level density formula with shell corrections, Can. J. Phys. 43 (8) (1965) 1446–1496.
[42] A. Blanc, A. Chebboubi, H. Faust, M. Jentschel, G. Kessedjian, U. Köster, T. Materna, S. Panebianco, C. Sage, W. Urban, FIssion product prompt γ-ray spectrometer: development of an instrumented gas-filled magnetic spectrometer at the ILL, Nucl. Instrum. Meth. B 317 (0) (2013) 333–337.